Simultaneous Binding of Drugs with Different Chemical Structures to Ca^{2+}-Calmodulin: Crystallographic and Spectroscopic Studies[†,‡]

Beata G. Vertessy,[§] Veronika Harmat,[∥] Zsolt Böcskei,[∥,⊥] Gábor Náray-Szabó,[∥] Ferenc Orosz,[§] and Judit Ovádi*[,§]

Institute of Enzymology, Biological Research Center, Hungarian Academy of Sciences, Department of Structural Chemistry, Eötvös Loránd University, and Chinoin Pharmaceuticals, Budapest, Hungary

Received April 9, 1998; Revised Manuscript Received July 13, 1998

ABSTRACT: The modulatory action of Ca^{2+}-calmodulin on multiple targets is inhibited by trifluoperazine, which competes with target proteins for calmodulin binding. The structure of calmodulin crystallized with two trifluoperazine molecules is determined by X-ray crystallography at 2.74 Å resolution. The X-ray data together with the characteristic and distinct signals obtained by circular dichroism in solution allowed us to identify the binding domains as well as the order of the binding of two trifluoperazine molecules to calmodulin. Accordingly, the binding of trifluperazine to the C-terminal hydrophobic pocket is followed by the interaction of the second drug molecule with an interdomain site. Recently, we demonstrated that the two bisindole derivatives, vinblastine and KAR-2 [3″-(β-chloroethyl)-2″,4″-dioxo-3,5″-spirooxazolidino-4-deacetoxyvinblastine], interact with calmodulin with comparable affinity; however, they display different functional effects [Orosz et al. (1997) British J. Pharmacol. 121, 955−962]. The structural basis responsible for these effects were investigated by circular dichroism and fluorescence spectroscopy. The data provide evidence that calmodulin can simultaneously accommodate trifluoperazine and KAR-2 as well as vinblastine and KAR-2, but not trifluoperazine and vinblastine. The combination of the binding and structural data suggests that distinct binding sites exist on calmodulin for vinblastine and KAR-2 which correspond, at least partly, to that of trifluoperazine at the C-terminal hydrophobic pocket and at an interdomain site, respectively. This structural arrangement can explain why these drugs display different anticalmodulin activities. Calmodulin complexed with melittin is also able to bind two trifluoperazine molecules, the binding of which appears to be cooperative. Results obtained with intact and proteolytically cleaved calmodulin reveal that the central linker region of the protein is indispensable for simultanous interactions with two molecules of either identical or different ligands.

The small acidic protein calmodulin (CaM)[1] can be considered as a main intracellular "switch" in many cellular processes controlled by Ca^{2+}-dependent signaling pathways. CaM controls the activity of several kinases and phosphatases, enzymes of cyclic nucleotide metabolism, and the Ca^{2+}-transport pump and interacts with the cytoskeleton (*1*, *2*). Mostly, CaM induces an increase in the activity of its target enzymes; however, in the case of the glycolytic enzyme 1-phosphofructokinase, enzymatic activity is decreased upon interaction with CaM (*3*, *4*). The crystal structure of CaM shows an elongated dumbbell-shaped molecule with two structurally similar globular domains separated by the central helix region (*5*−*7*); however, in solution this region is flexible (*8*, *9*). The protein can be selectively cleaved at residue Lys 77 of this segment by limited trypsinolysis (*10*). The resulting globular domains are homologous, and each contains a pair of the Ca^{2+}-binding helix−loop−helix motifs, termed EF-hands. Ca^{2+}-induced protein conformational changes lead to the exposure of hydrophobic surfaces on both domains, which are responsible for binding of various target peptides as determined by NMR spectroscopy in solution (*11*) or by X-ray crystallography (*12*, *13*).

Anti-CaM drugs of strikingly heterogeneous chemical structure prevent or modify the interactions of CaM with target enzymes. Presently, a detailed structural description of drug binding to CaM is available only in the case of trifluoperazine (TFP), a phenothiazine derivative. CaM has been crystallized with one and four TFP molecules, and the structures of CaM−drug complexes were determined at 2.45 or 2.0 Å resolution, respectively (*14*, *15*). Both crystal structures suggest a unique site for TFP binding in the C-terminal globular domain: this is the only site occupied in the 1:1 CaM−TFP complex, while this is the best-defined site in the 1:4 CaM−TFP complex (*14*, *15*). In the latter structure two TFP molecules are accommodated at the sequentially homologous hydrophobic pockets of the C- and

[†] This study was supported by grants from the Hungarian National Science Foundation and the Ministry for Education: OTKA F-017392 and F-020862 to B.G.V., T-17830 and T-025291 to J.O., and T-022191 to G.N.-S.

[‡] X-ray structural data have been deposited in the Brookhaven Protein Data Bank under Accession Number 1a29.

* Correspondence should be addressed to this author at the Hungarian Academy of Sciences, P.O. Box 7, H-1518, Budapest, Hungary. Phone: +361 1665 923. Fax: +361 1665 465. E-mail: ovadi@enzim.hu.

[§] Hungarian Academy of Sciences.

[∥] Eötvös Loránd University.

[⊥] Chinoin Pharmaceuticals.

[1] Abbreviations: CaM, calmodulin; TFP, trifluoperazine; KAR-2, 3″-(β-chloroethyl)-2″,4″-dioxo-3,5″-spirooxazolidino-4-deacetoxyvinblastin; CD, circular dichroism.

10.1021/bi980795a CCC: $15.00
Published on Web 10/20/1998

N-terminal halves, termed as "intradomain sites", while the other two TFP molecules were found at the central linker region termed as "interdomain sites".

In contrast to the crystal structure data, several solution studies indicate that the primary two or four (five) phenothiazine binding sites on intact CaM display commeasurable affinities (*16*−*18*). Photolabeling of CaM with a reactive phenothiazine derivative indicated two binding sites, one in each globular domain (*19*). Another chemically reactive derivative labeled only the C-terminal domain when applied at low molar ratios (*20*). ^{1}H NMR data also suggested a first unique site which elicits distinct signals, although this site was not localized to the C-terminal domain (*21*).

Our previous data suggested that fendiline and other arylalkylamine derivatives, and several bisindole drugs with different structural and pharmacological properties, interact with CaM, with an affinity comparable to that of TFP binding (*22*−*24*). The bisindole derivatives vinblastine and navelbine, extensively used in tumor chemotherapy, display a Ca^{2+}-dependent anti-CaM potency by a competitive mechanism (*23*, *25*). A novel bisindole analogue, 3″-(*β*-chloroethyl)-2″,4″-dioxo-3,5″-spirooxazolidino-4-deacetoxyvinblastine (KAR-2), in contrast to most of the CaM antagonists, interacts with CaM, but it does not affect CaM action on the glycolytic enzyme 1-phosphofructokinase (*26*). Another distinguishing feature of KAR-2 is that it binds to CaM even in the absence of Ca^{2+} and renders apoCaM crystallizable (*27*). Experiments with tumor cell lines revealed that KAR-2 is efficient in killing malignantly transformed cells, while its effect on normal cells is much less toxic compared to the other bisindole drugs vincristine and vinblastine (*28*). A principal objective of these studies is to characterize the relationship of the binding sites of drugs responsible for distinct functional effects.

Melittin, an active ingredient of bee venom, is a 26-residue peptide antagonist of CaM (*29*, *30*). It binds to the protein with a nanomolar dissociation constant, i.e., approximately 1000-fold stronger than either TFP or bisindoles. Although a high-resolution structure of the melittin−CaM complex is not yet available, the data obtained from experiments in solution indicate that melittin, similarly to other target peptides, interacts with both the N- and C-terminal domains (*31*, *32*). In addition, it has multiple contacts to the interdomain sites at the central linker region of the intact CaM, and complexation involves both hydrophobic and electrostatic forces (*32*, *33*). TFP binding to the CaM−melittin complex has been demonstrated by gel filtration experiments (*18*). Previously, we suggested a combined binding of TFP and a neuropeptide which has characteristics similar to that of melittin in many respects (*34*). Further possibilities for ternary complex formation among CaM and two different ligands are also worthwhile to investigate for identification of the multiple binding sites.

In the present work, we carried out experiments on CaM−TFP complexes simultaneously in crystal by X-ray crystallography and in solution by near-UV circular dichroism (CD) spectroscopy. These studies allowed us to determine the order of occupation of the first two TFP binding sites on the protein, which may resolve the discrepancy among the data from the literature. We investigated the possibility that the different binding sites are simultaneously occupied by different ligands. Ternary mixtures of CaM and TFP, bisindoles, and/or melittin were studied by CD and fluorescence spectroscopy. The distinct spectroscopic signals obtained by the binding of drugs with different chemical structure to the intact and trypsinolyzed CaM rendered it possible to characterize the binary and ternary CaM−drug complexes and the role of the central linker region in complexation. In addition, the pharmacological effects of the drugs with different chemical structures are interpreted on the basis of the structural data.

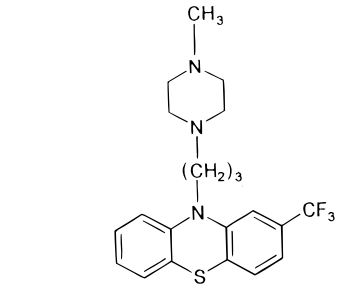

Trifluoperazine

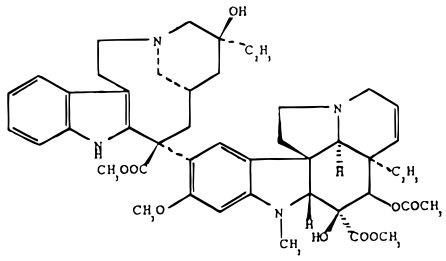

Vinblastine

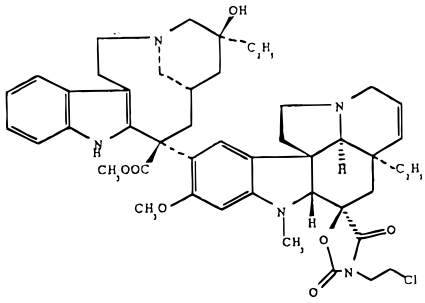

KAR-2

FIGURE 1: Structural formulas of trifluoroperazine, vinblastine, and KAR-2.

EXPERIMENTAL PROCEDURES

Chemicals. The bisindoles vinblastine and KAR-2 were kindly provided by Chemical Works of Gedeon Richter Ltd., Budapest. The structure of KAR-2 (Figure 1) was supported by its ^{13}C NMR, ^{1}H NMR, IR, and mass spectra (*24*). Dansyl-CaM, trypsin, trypsin inhibitor, melittin, TFP, and buffer substances were purchased from Sigma. All other chemicals were reagent-grade commercial preparations. CaM from bovine brain was purified using Phenyl-Sepharose (Pharmacia) chromatography (*35*). Protein purity was determined by discontinuous polyacrylamide gel electrophoresis in the presence of sodium dodecyl sulfate (*36*).

CaM Concentration. This was determined spectrophotometrically using a molar absorption coefficient of 3.24×10^3 M^{-1} cm^{-1} at 276 nm (*37*) or by CD spectroscopy using the molar residual ellipticity of 15 800 deg cm^2 $dmol^{-1}$ at

222 nm (*27*). For spectrophotometric measurements HP 8451A or JASCO V-550 spectrophotometers were used.

Fluorescence Measurements. Fluorescence studies were conducted on a JASCO Model FP-777 spectrofluorometer, using excitation and emission slits of 3 nm. Fluorescence excitation and emission spectra of dansyl-CaM and Vinca alkaloids were measured at 25 °C in a buffer containing 10 mM 3-(*N*-morpholino)propanesulfonic acid (MOPS), pH 7.0, 90 mM KCl, 2 mM ethylene glycol bis(*β*-aminoethyl ether)-*N*,*N*,*N*′,*N*′-tetraacetic acid (EGTA), and 3 mM $CaCl_2$. The excitation wavelength of dansyl-CaM was 340 nm. Spectra were corrected for inner filter effects according to

$$F_{corr} = F_{obs}[10^{(OD_{ex}+OD_{em})/2}]$$

where OD_{ex} and OD_{em} refer to the optical density of the sample (38).

Circular Dichroism Measurements. Circular dichroism spectra were recorded with a JASCO J-720 spectropolarimeter. Measurements were done at 25 °C in thermostated cuvettes in 50 mM piperazine-*N*,*N*′-bis(2-ethanesulfonic acid) (PIPES), 100 mM KCl, 1 mM ethylene glycol bis(*β*-aminoethyl ether)-*N*,*N*,*N*′,*N*′-tetraacetic acid (EGTA), and 5 mM $CaCl_2$, pH 6.8, buffer. For measurement of ligand−protein mixtures, ligand was added to the protein solution, the solution was mixed, and circular dichroism spectrum was recorded in the 240−360 nm wavelength range. Scanning was repeated twice, and the spectra were averaged. Spectra measured immediately after mixing were stable for at least 20 min; i.e., complex formation was complete in 2−5 min at the concentrations used in our experiments. In the case of ternary mixtures, the order of the addition of the different ligands was found to exert no effect on the resulting spectra; i.e., the binding/dissociation processes reached thermodynamic equilibrium during the incubation time. Spectrum averaging and mathematical operations were performed using the built-in software of the instrument. No difference spectrum was obtained in the absence of protein if any two of the ligands TFP, vinblastine, KAR-2, or melittin were mixed; the spectra of these mixtures were identical to the sum of the spectra of the components measured separately. This observation corroborates the CD difference signals obtained in the ternary mixtures of the protein with two ligands to describe the interaction of the protein with the ligands.

Limited Tryptic Digestion of CaM. CaM was digested by trypsin as previously described (*34*) following the original report of Walsh et al. (*10*). Briefly, 120 *μ*M CaM in 10 mM piperazine-*N*,*N*′-bis(2-ethanesulfonic acid) (PIPES) and 0.2 mM $CaCl_2$, pH 6.5, buffer was digested with 0.04 mg/mL trypsin for 60 min at 30 °C, and the reaction was stopped by the addition of 0.12 mg/mL trypsin inhibitor. Fragments were analyzed by gel electrophoresis in the presence of sodium dodecyl sulfate (*36*) on 16% polyacrylamide gels.

Crystallization and X-ray Diffraction. Crystallization trials were conducted using the vapor diffusion hanging drop (bridges from Crystal Microsystems, Cambridge, U.K.) technique in the cold room (8 ± 2 °C). Crystals suitable for X-ray diffraction were obtained by mixing 4 *μ*L of 1 mM protein containing 1.2−1.7 mM TFP in 5 mM $CaCl_2$ with 4 *μ*L of the reservoir solution [1 mL of 10 mM sodium cacodylate/HCl buffer, pH 5.2, with 10 mM $CaCl_2$ and 30% (w/v) poly(ethylene glycol) 6000]; crystal growth took 2−3 weeks. X-ray data were collected in 25 oscillation frames at room temperature using a Rigaku R-AXIS IIC imaging plate detector attached to a Rigaku RU-H2R rotating anode generator. All data were collected from one crystal of space group $P3_221$ with cell constants $a = b = 40.75(2)$ Å and $c = 177.57(5)$ Å, isostructural with the two calmodulin−TFP complexes found in the literature (*14*, *15*). A total of 12 467 reflections (5036 independent reflections, 95.1% complete to 2.74 Å resolution) were measured with an R_{sym} of 0.0737. The data were processed using the BioteX program package (*39*). The structure was determined by molecular replacement using the AMoRe program (*40*) of the CCP4 package, with the protein part of the CaM−4TFP complex. During molecular replacement the molecule was treated as a single rigid body. The model building steps were carried out with the O program (*41*). The resulting model was refined with the program X-PLOR, version 3.851 (*42*). We used torsion angle dynamics (*43*−*45*) (first refinement cycle, slow cooling from 4000 K) or molecular dynamics (*46*−*48*) (all other refinement cycles, slow cooling from 3000 K), resolution-dependent weighting, overall anisotropic *B*-factor refinement, bulk solvent correction (*49*), and grouped *B*-factor refinement during the refinement. $R = 0.197$, $R_{free} = 0.265$ for reflections with $F_o > 2.0\sigma(F_o)$ at the end of the final refinement. The final structure consists of 144 amino acid residues of calmodulin, 4 calcium ions, and 2 TFP molecules; it has root-mean-square deviations of 0.006 Å in bond lengths and 1.08° in bond angles and an average temperature factor of 30.04 Å^2 for 1147 atoms.

RESULTS AND DISCUSSION

Subsequent Distinct Saturation of TFP Binding Sites Monitored by Differential Near-UV CD Spectroscopy. CD spectroscopy in the near-ultraviolet wavelength range is considered to be one of the most sensitive methods to follow fine changes in the tertiary protein conformation induced by ligand binding. Characteristic spectra for the binding of TFP to trypsinolyzed CaM (*50*) and for binding of bisindole drugs to intact CaM (*23*, *26*) have been reported. Figure 2 shows the difference CD spectra of intact and trypsin-digested CaM (20 *μ*M) measured in the presence of increasing TFP concentrations. At low TFP concentrations, a characteristic negative difference peak is formed at 263 nm reaching saturating value (Figure 2A). This saturation displays hyperbolic character (cf. Figure 2A inset); the apparent dissociation constant and the number of ligand binding sites in the CaM−TFP complex are 1.0 *μ*M and 0.72. When this titration is repeated at a higher (150 *μ*M) protein concentration in order to provide more reliable stoichiometric data, the same stoichiometry is found (Figure 2A inset). These data strongly suggest that there is one well-defined, unique TFP binding site on CaM, the saturation of which causes a negative difference CD peak at 263 nm. Further increases in TFP concentration result in a continuous blue shift of the negative peak with the concomitant appearance of a positive peak at 270 nm (Figure 2A). The observation that the negative and positive CD signals form consecutively during the TFP titration indicates that there is more than one distinct TFP binding site on the intact CaM.

To investigate the possible role of the central linker region of CaM in the development of these TFP binding-induced

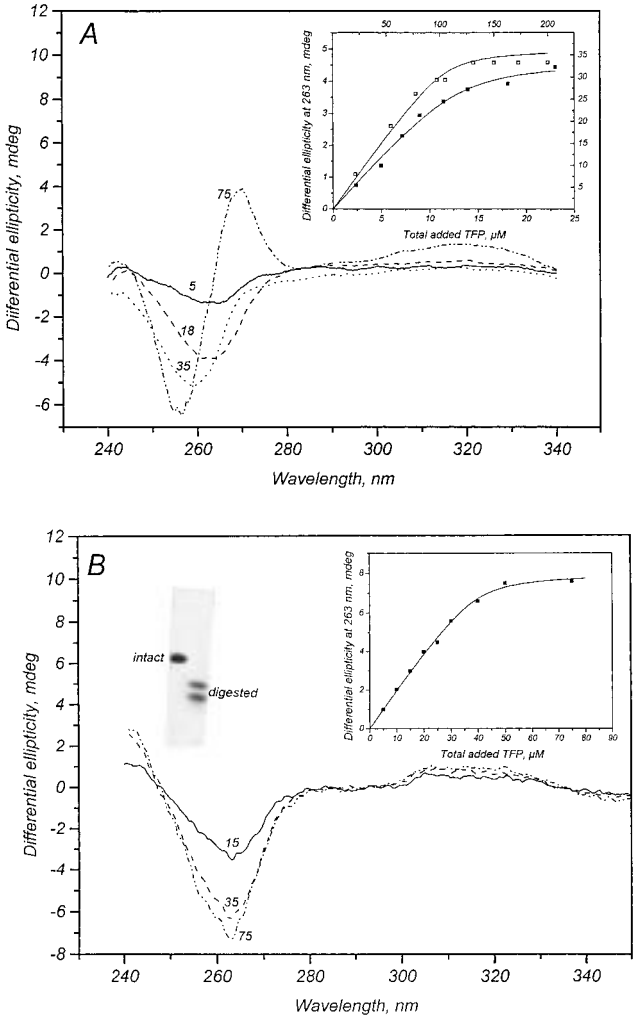

FIGURE 2: Binding of TFP to intact (A) and trypsinolyzed (B) CaM as followed by near-UV CD difference spectra was calculated by subtracting the spectrum of CaM from the spectrum measured in the mixture. TFP alone does not have any signal in this wavelength range. (A) Difference spectra of 20 μM CaM and TFP at concentrations indicated on the spectra in μM. (Inset to panel A) Titration of 20 μM CaM (closed symbols, bottom and left axes) or 150 μM CaM (open symbols, right and top axes) is shown. The solid lines are fitted curves to the equation [assuming identical and independent binding site(s)] (*53*) $\Delta\Theta = (K_d/(2(1/[\Theta]^2)))(((cn/[\Theta]/K_d) + [TFP]/[\Theta]/K_d + 1/[\Theta]) - (((cn/[\Theta]/K_d) + [TFP]/[\Theta]/K_d + 1/[\Theta])^2 - (4((1/[\Theta])^2)/K_d[TFP]cn/K_d))^{0.5})$, where $\Delta\Theta$ = differential ellipticity at 263 nm as shown on the ordinate, $[\Theta]$ = molar ellipticity of the complex, n = number of ligands bound per number of macromolecules, K_d = apparent dissociation constant, c = macromolecule concentration, and [TFP] = TFP concentration as shown on the abscissa. For the data set with 20 μM CaM, $[\Theta] = 357 \pm 42$ deg/M/cm, $n = 0.72 \pm 0.05$, $K_d = 1 \pm 0.6$ μM, $c = 20$ μM, and $\chi^2 = 3.1 \times 10^{-8}$. For the data set with 150 μM CaM, $[\Theta] = 345 \pm 41$ deg/M/cm, $n = 0.72 \pm 0.08$, $K_d = 1.8 \pm 0.8$ μM, $c = 150$ μM, and $\chi^2 = 7.2 \times 10^{-8}$. (B) Difference spectra of 20 μM digested CaM and TFP at concentrations indicated on the spectra in μM. The photographs of the gel lanes show the intact (single band) and 60-min-digested (double bands reflecting the C- and N-terminal fragments) CaM samples. (Inset to panel B) The titration data were fitted as described above for the intact CaM with parameters $[\Theta] = 222 \pm 50$ deg/M/cm, $n = 1.9 \pm 0.3$, $K_d = (1.6 \pm 0.7)$ μM, $c = 20$ μM, and $\chi^2 = 2.6 \times 10^{-8}$.

characteristic CD signals, similar titration experiments were carried out with trypsin-digested CaM. Under limiting conditions, CaM is cleaved at the central linker region (residue 77), producing N- and C-terminal fragments with folded globular structure similar to that of the intact protein (*10*). In the experiment presented in Figure 2B, the fragments were not separated; however, the covalent connection between them was abolished by limited proteolysis. Titration of the mixture of fragments with TFP leads to the appearance of a single negative peak at 263 nm, and no second, positive peak appears even at the highest TFP concentration used in the case of intact CaM (cf. Figure 2B). The saturation curve (Figure 2B inset) can be well described by assuming identical and independent binding sites with an apparent dissociation constant of 1.6 μM and approximately two (1.9) binding sites.

Qualitative evaluation of the difference signals shows that the negative difference peak of the digested protein−TFP complex exhibits characteristics similar to those of the negative CD signal formed at the beginning of the titration of intact CaM (cf. Figure 2A). This finding suggests that in both cases similar binding sites are saturated by TFP. However, the extent of the negative CD signal is enhanced (ca. double) in the experiment performed with digested CaM. In the titration with intact CaM, a positive difference peak is also elicited at 270 nm, arguing for a different binding pattern.

We interpret these qualitative results in the light of the crystal structural data of the CaM−TFP complex (*14*, *15*) in the following way. In the 1:4 CaM−TFP complex structure two different types of TFP binding sites have been identified, referred to as intradomain and interdomain sites. The one−one intradomain site is localized in both C- and N-terminal globular domains. The amino acid residues participating in ligand accommodation at these intradomain sites are residues closely related by sequence homology. Since these two intradomain sites are very similar concerning the amino acid residues involved in TFP binding, it can be expected that the binding of the drug to these sites elicits similar spectral changes: this is the negative CD signal with a minimum at 263 nm. However, if TFP molecules are accommodated at the interdomain sites stabilized by different interacting forces, one can expect that the binding probably induces different spectral signals. Therefore, we hypothesize that the positive CD signal appearing at high TFP concentrations corresponds to the binding of TFP to an interdomain site. This structural arrangement can explain why the mixture of CaM fragments does not produce a positive CD signal even at high TFP concentrations (because interdomain sites are not available in the fragments due to the proteolytic cleavage). Quantitatively, the saturation curve of the trypsinolyzed CaM could be fitted by assuming that two drug molecules are bound, presumably one to each intradomain site (Figure 2B inset). Clearly, disruption of the central linker region modifies TFP binding: the C- and N-terminal intradomain sites become saturated as equal and independent sites. Nevertheless, it is not clear from the spectroscopic titration data whether the appearance of a positive difference CD signal during TFP titration of intact CaM is due to the binding of TFP to only an interdomain site or whether the N-terminal hydrophobic pocket also gets occupied. To get an unambiguous answer to this question, a high-resolution structure was sought.

Crystal Structure of CaM Complexed with Two TFP Molecules: The Second Site Is an Interdomain Site. Localization of the second binding site was attempted by X-ray crystallography. Crystals were grown at a 1.2:1.7 TFP:CaM

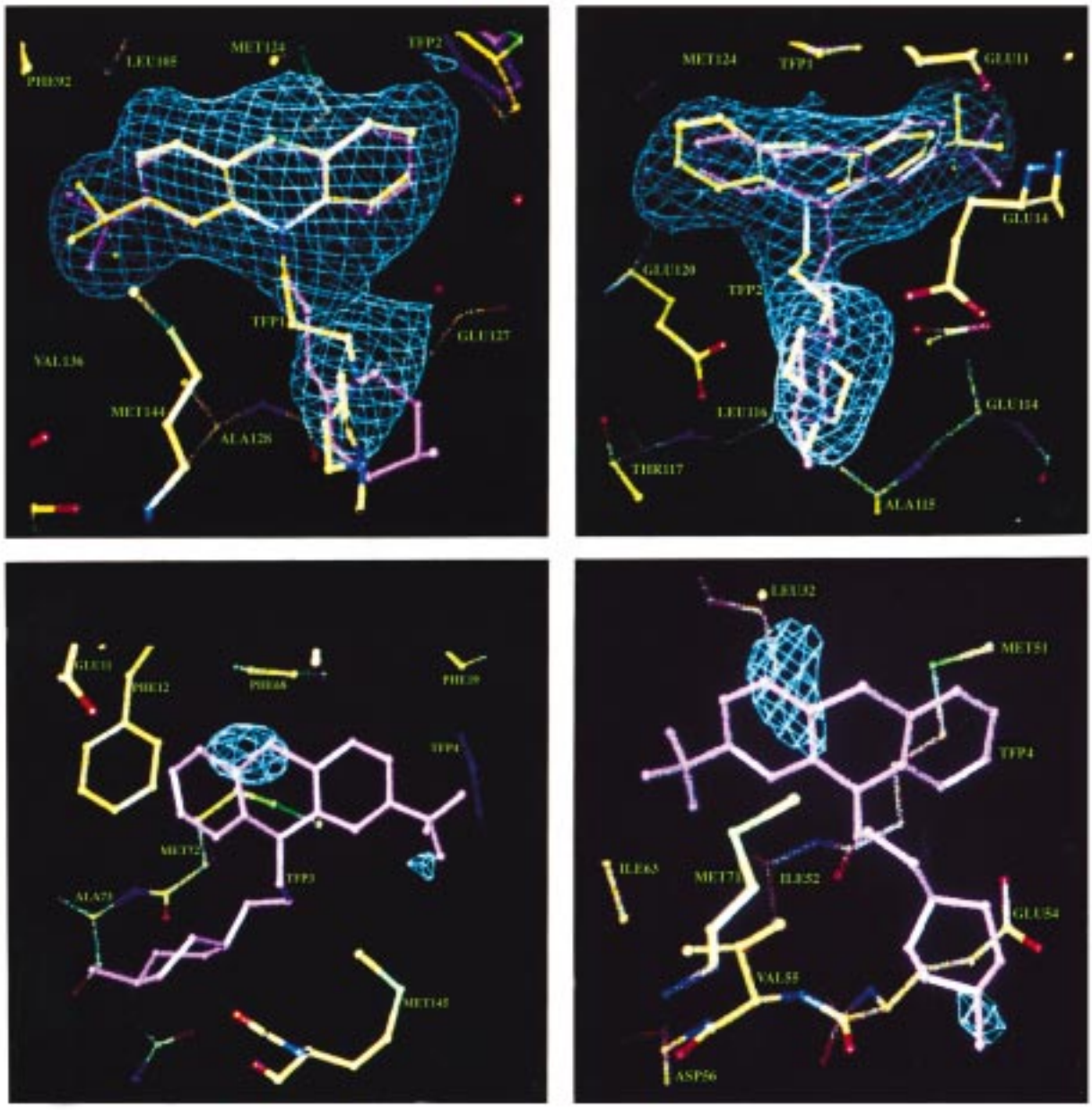

FIGURE 3: Binding of the two TFP molecules to CaM as determined by X-ray crystallography. The 2.74 Å resolution refined model (yellow, carbon; red, oxygen; blue, nitrogen; green, sulfur and fluor atoms) and $F_o - F_c$ omit electron density map (cyan, 3σ contour) calculated without the two TFP molecules are shown at the binding sites of TFP1 (panel A, top left), TFP2 (panel B, top right), TFP3 (panel C, bottom left), and TFP4 (panel D, bottom right) molecules (magenta) of the CaM−4TFP complex (*15*). The TFP molecules fitted into the electron density map determined in the present study are colored yellow at sites TFP1 and TFP2 (panels A and B).

ratio; data collection statistics are given in Experimental Procedures. The structure is well-defined by the electron density apart from a few surface side chains and the residues of the central region. In the final model, residues 74−80 which possess a weak electron density map as well as residues 6, 7, 53, 84, 87, 94, and 115 which have weak side chain densities are all modeled as alanines, while residues 1, 2, 147, and 148 are missing. The overall conformation of calmodulin is similar to that of the CaM−1TFP (*14*) and CaM−4TFP (*15*) complexes; the root-mean-square deviations of the backbone atoms are 0.734 Å (for 552 atoms) and 0.426 Å (for 576 atoms), respectively. We identified two TFP molecules at sites corresponding to TFP1 and TFP2 of the CaM−4TFP structure (Figure 3A, B). TFP1 is bound in the hydrophobic pocket of the C-terminal domain of CaM while TFP2 occupies an interdomain site. At the positions of TFP3 (another interdomain site) and TFP4 (the N-terminal intradomain site) there is no appreciable electron density in our structure (Figure 3C, D). The orientation of the tricyclic ring and the trifluoro group of TFP1 is nearly the same as in the CaM−4TFP structure. This is in contrast to the CaM−1TFP complex structure where the tricyclic ring of TFP is inverted and is in a 180° rotated position. Comparing the binding site of TFP2 in our structure with that in the CaM−4TFP complex, we find some minor differences. TFP2 in our structure is slightly shifted toward helix G and it makes a hydrogen bond with the side chain of Glu 127 [the distance between N2(TFP2) and OE2(Glu120) is 3.21 Å]. In the conformation of the piperazine rings of the TFP molecules there is a greater variance among the three complexes as these parts of the molecules are more solvent exposed. It should be pointed out that the TFP1 and TFP2 sites occupied

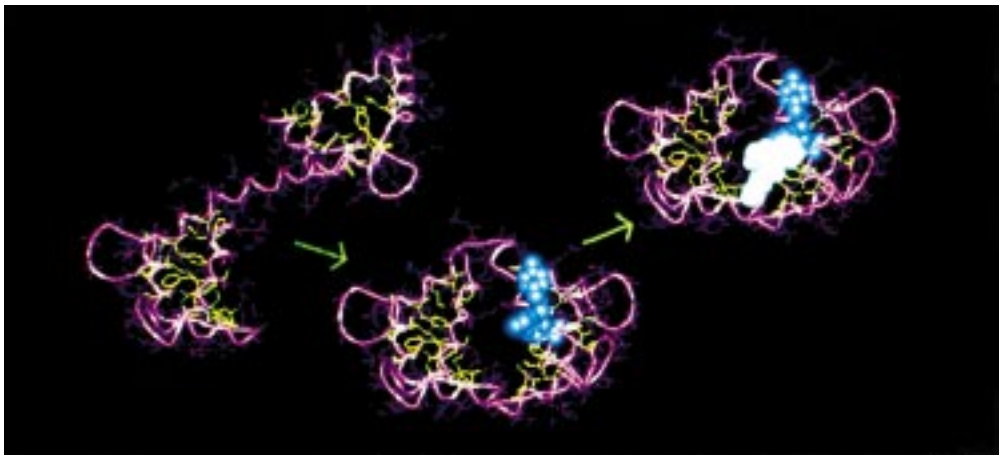

FIGURE 4: Order of saturation of the first two TFP binding sites on Ca2+-CaM. The first TFP molecule (blue) binds to the hydrophobic pocket of the C-terminal domain, and the second (white) occupies an interdomain site. The Cα chain of the protein is colored magenta, and amino acid residues involved in TFP binding at the intradomain hydrophobic pockets are shown in yellow.

in our structure correspond to the two best-defined sites in the study of Vandonselaar et al. (*15*).

The combination of the CD data in solution and the X-ray data in crystal for the CaM−TFP complex allowed us to construct a schematic model of subsequent saturation of intra- and interdomain sites of the intact CaM by TFP molecules (Figure 4). The hydrophobic pocket in the C-terminal domain is the first to get occupied, followed by an interdomain site. This model reveals an indispensable role of the central linker region in the accommodation of the second TFP molecule in intact CaM. The data in Figure 1B also suggested that, after cleavage at the central linker, the N- and C-terminal intradomain sites become equal and independent sites which may bind one TFP molecule each.

CaM Is Able To Form Ternary Complexes with Two Different Ligands. Bisindoles and TFP. The binding of KAR-2 or vinblastine to CaM also induces CD difference spectra with a characteristic negative peak around 300 nm (*26*). In the case of vinblastine there is an additional positive difference peak with a maximum at 262 nm (*26*). The interactions of these bisindoles with CaM were quantified by fluorescence spectroscopic analysis (*23*, *26*): the dissociation constants were 5.2 μM and 3.0 μM for KAR-2 and vinblastine, respectively, assuming 1:1 stoichiometry. Since we found that in the range of 300−350 nm TFP binding to CaM does not produce a significant signal, the binding of bisindoles can be conveniently monitored in the presence of TFP in this wavelength range.

Figure 5 presents the difference CD spectra of the mixtures of CaM and TFP in the presence of KAR-2 (Figure 5A) or vinblastine (Figure 5B). In the first set of experiments, the TFP concentration was chosen to be nearly equimolar to CaM. Under this condition predominantly the first TFP site (eliciting the negative CD signal at 263 nm; cf. Figure 2A) gets occupied. To identify the mechanism of binding of the two drugs with different chemical structures to CaM, theoretical spectra were computed using the spectra of binary complexes and compared with the experimental data measured in the presence of TFP and one of the bisindoles. It was assumed that the shape and extent of CD signals (molar ellipticity coefficients) characteristic for the binding of drugs were the same within the binary and ternary complexes. The following mechanisms were considered:

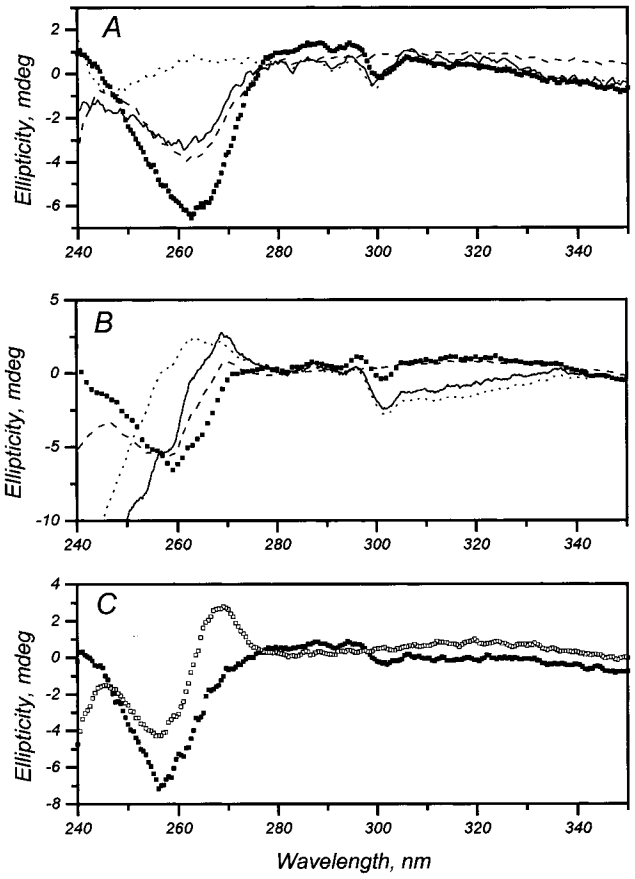

FIGURE 5: Mutual effects of TFP and bisindoles on their binding to CaM as detected by near-UV CD. (A and B) Difference spectra (scattered graphs of closed squares) were calculated by subtracting the spectra of the components measured alone from the spectrum measured in their mixture. Theoretical curves corresponding to the cases discussed in the text were calculated as follows. The solid line is the sum of the difference spectra measured with CaM−TFP and CaM−bisindole binary mixtures (case A). The dashed line is the difference spectrum of the CaM−TFP binary mixture (case B_1 with no bisindole binding). The dotted line is the difference spectrum of the CaM−bisindole binary mixture (case B_2 with no TFP binding). Concentrations: panel A, 20 μM CaM, 31.2 μM TFP, and 30 μM KAR-2; in panel B, 20 μM CaM, 30 μM TFP, and 30 μM vinblastine. (C) Difference spectra of 20 μM CaM and 60 μM TFP in the absence (open squares) or presence (closed squares) of 60 μM KAR-2.

case A, independent (simultaneous) binding of TFP and KAR-2/vinblastine to CaM; case B, competitive (alternative) binding of TFP and KAR-2/vinblastine to CaM. With case B_1 only TFP binds and with case B_2 only KAR-2/vinblastine binds to the protein in the ternary mixtures.

The comparison of the computed and measured spectra shows that in 300−350 nm range, characteristic for bisindole binding, the measured difference spectrum displays a negative peak at 300 nm to the same extent as the computed curves for case A or case B_2 when the experiment is performed with KAR-2 (Figure 5A). This result suggests that KAR-2 binding is not perturbed in the ternary mixture. However, when vinblastine is used instead of KAR-2, the signal of the measured difference spectrum in the 300−350 nm wavelength range is much less enhanced than in the computed curves for case A or case B_2 (Figure 5B), arguing for the interpretation that vinblastine binding to the protein is significantly decreased in the presence of TFP. We conclude that in the CaM−TFP−bisindole mixture KAR-2 may bind to the protein; however, the interaction of vinblastine with CaM is practically abolished by TFP.

When the computed and measured spectra were analyzed in 255−275 nm range, characteristic for TFP binding, we found that in the presence of KAR-2 the difference signal is significantly enhanced. This enhancement suggests ternary CaM−TFP−KAR-2 complex formation. Since it cannot be described by the model curve constructed for case A, cooperative binding of the two drugs is suggested. In the case of vinblastine the measured spectrum is similar to that obtained for case B_1.

We conclude that TFP and KAR-2 interact simultaneously with CaM, while vinblastine is not able to bind to the CaM−TFP complex. In light of the data from Figures 2−4, one can hypothesize that the C-terminal hydrophobic pocket of CaM can alternatively accommodate TFP or vinblastine; however, KAR-2 may have at least a partly distinct binding domain. To test the role of interdomain sites in KAR-2 binding and whether the binding of the second TFP to CaM interferes with KAR-2, KAR-2 was added to a CaM−TFP mixture which exhibits both negative and positive difference CD signals (i.e., both intra- and interdomain TFP sites are occupied; cf. Figure 2). Figure 5C shows that KAR-2 increased the negative differential ellipticity peak but completely erased the positive one. In addition, a new negative signal appeared at 300 nm due to the binding of KAR-2 to CaM. On one hand, the fact that the signal of the first TFP binding is not diminished but enhanced by KAR-2 suggests again formation of a ternary complex. On the other hand, KAR-2-induced decrease in the positive signal at 270 nm may be interpreted by direct or indirect competition between KAR-2 and TFP for the interdomain site.

Similar experiments were also performed with trypsin-digested CaM plus TFP and KAR-2. In this case the presence of KAR-2 caused a significant decrease in the TFP binding-induced peak at 263 nm and titration experiments could be interpreted by competition between these two drugs for CaM binding, with no indication for ternary complex formation (data not shown). We conclude that the central linker region is essential for the ternary complexation. Scheme 1 was constructed on the basis of the above data. Distinct intra- and interdomain sites are suggested to exist: one TFP molecule and vinblastine occupies intradomain sites, while binding of the second TFP or KAR-2 involves an interdomain site.

Scheme 1: CaM−Ligand Interactions in CaM−TFP−Bisindole Ternary Mixtures, Constructed from Data Obtained by CD and Fluorescence Spectroscopy and X-ray Crystallography[a]

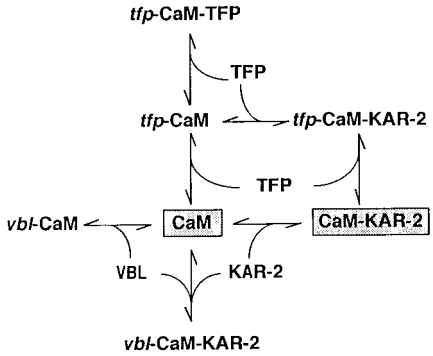

[a] VBL stands for vinblastine. Ligands depicted in italic type are presumably bound to the C-terminal hydrophobic intradomain site of CaM. CaM in stippled rectangles possesses functional activity in the phosphofructokinase test (*26*).

Simultaneous Binding of KAR-2 and Vinblastine to CaM. CD measurements indirectly suggested that CaM may use different binding patterns for the two bisindoles (cf. Scheme 1). In this case KAR-2 and vinblastine may be able to bind simultaneously to CaM. Since the binding of both drug molecules induces similar CD signals (Figure 5) and their affinity toward CaM is also similar (*23*, *26*), another technique was explored to study the presumed ternary complex of CaM and the two bisindoles. We designed fluorescence experiments to monitor the binding of one of two in the presence of the other.

Johnson and Wittenauer (*51*) showed that the binding of several CaM antagonists dramatically (by 60%−90%) enhances the fluorescence emission of dansyl-labeled CaM when excited at 340 nm. We measured the effect of KAR-2 and vinblastine on the fluorescence emission spectrum of dansyl-CaM. On one hand, the fluorescence emission spectrum of dansyl-CaM was perturbed by KAR-2: the maximum of the free dansyl-CaM from 505 nm was blue-shifted to 473 nm and the fluorescence intensity at 473 nm was enhanced by 60% by addition of excess KAR-2 (Figure 6A). On the other hand, vinblastine perturbed only slightly (10%) the fluorescence emission spectrum of dansyl-CaM (*23*). Neither drug emits fluorescent light when excited at 340 nm.

The observation that the interaction of KAR-2 but not vinblastine with CaM induces significant alteration in the fluorescence intensity of dansyl-CaM renders it possible to decide if the two bisindoles bind simultaneously or alternatively to CaM. Fluorescence intensity of dansyl-CaM was measured at 473 nm as a function of KAR-2 concentration in the absence and presence of excess vinblastine. As shown in Figure 6B KAR-2 increases the fluorescent intensity of dansyl-CaM reaching a nearly saturating value. The dissociation constant calculated from this curve (Figure 6B, curve a), assuming hyperbolic saturation of CaM with KAR-2 and a single binding site, was 4.6 ± 0.3 μM. This value is in good agreement with the one determined previously by fluorescence energy transfer measurements (5.2 ± 0.6 μM) (*26*).

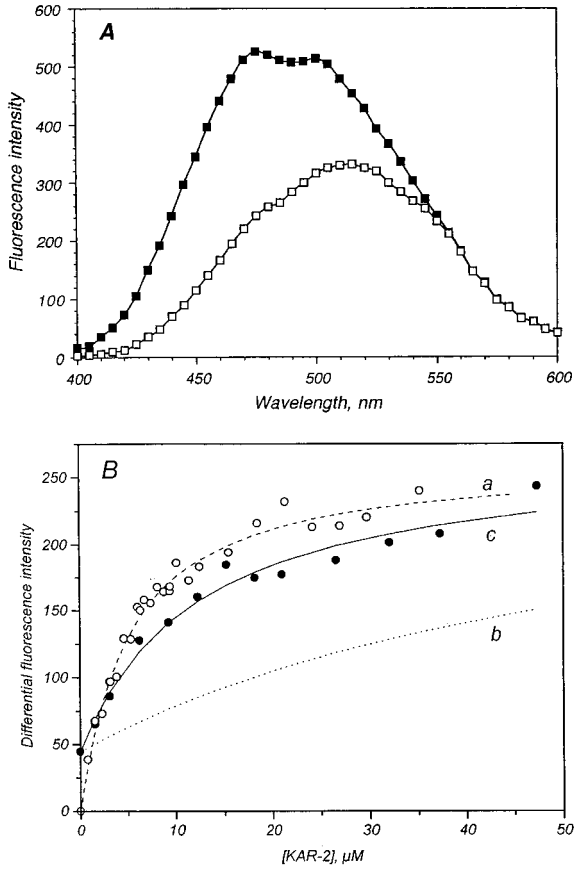

FIGURE 6: (A) Effect of KAR-2 on dansyl-CaM fluorescence. The fluorescence intensity of dansyl-labeled CaM was measured at an excitation wavelength of 340 nm. Lines show emission spectra of 1.08 μM dansyl-CaM in the absence (open squares) and in the presence (closed squares) of 20 μM KAR-2. (B) Titration curve of dansyl-CaM (1.08 mM) with KAR-2 in the absence (open symbols) and presence (closed symbols) of vinblastine (36 μM). The fluorescence increase at 473 nm is shown as a function of added KAR-2. Lines are theoretical curves calculated by numerical integration of the following equations:

$$[\text{CaM}][\text{VBL}]/[\text{CaM}-\text{VBL}] = K_1 \quad (1)$$

$$[\text{CaM}][\text{KAR-2}]/[\text{CaM}-\text{KAR-2}] = K_2 \quad (2)$$

$$[\text{CaM}-\text{VBL}][\text{KAR-2}]/[\text{VBL}-\text{CaM}-\text{KAR-2}] = K_3 \quad (3)$$

$$[\text{VBL}]_{\text{total}} = [\text{VBL}] + [\text{CaM}-\text{VBL}] + [\text{VBL}-\text{CaM}-\text{KAR-2}] \quad (4)$$

$$[\text{KAR-2}]_{\text{total}} = [\text{KAR-2}] + [\text{CaM}-\text{KAR-2}] + [\text{VBL}-\text{CaM}-\text{KAR-2}] \quad (5)$$

$$[\text{CaM}]_{\text{total}} = [\text{CaM}] + [\text{CaM}-\text{VBL}] + [\text{CaM}-\text{KAR-2}] + [\text{VBL}-\text{CaM}-\text{KAR-2}] \quad (6)$$

$$\Delta\text{FI} = \alpha[\text{CaM}-\text{VBL}] + \beta[\text{CaM}-\text{KAR-2}] + \gamma[\text{VBL}-\text{CaM}-\text{KAR-2}] \quad (7)$$

where K_1, K_2, and K_3 are apparent dissociation constants, ΔFI is the measured change in fluorescence intensity, α, β, and γ are the maximal changes in fluorescence intensity at saturating ligand concentration, and VBL is vinblastine. K_1 (3.0 μM) and α (44.5) were taken from independent measurements (*23*). Theoretical curves were computed according to the method of ref *54* for the following cases. The dashed line (curve a) assumes 1:1 CaM−KAR-2 complexation (without vinblastine), with best fit parameters $K_2 = 4.6 \pm 0.3$ μM and $\beta = 243$. These parameters were fixed for further calculations. The dotted line (curve b) assumes CaM−KAR-2 and CaM−vinblastine complexes (no ternary complex formation). The solid line (curve c) assumes ternary complex formation, with best fit parameters $K_3 = 15.3$ μM and $\gamma = 259$.

The presence of vinblastine (36 μM) significantly reduces the enhancement of fluorescent intensity. Two alternative mechanisms can be responsible for this qualitative effect: (i) the two bisindoles compete for binding to CaM; therefore, their bindings are alternative; (ii) the two bisindoles bind simultaneously to CaM; however, the affinity of KAR-2 is reduced within the ternary complex. We have evaluated quantitative models for these two alternatives (see equations in the legend to Figure 6).

Using the dissociation constants of the binary complexes [3.0 μM and 4.6 μM for vinblastine (*23*) and KAR-2 (from curve a) binding, respectively], the competitive (alternative) model can be excluded as shown by the theoretical dotted curve on Figure 6B (curve b). The solid line is a theoretical curve calculated assuming simultaneous binding for KAR-2 and vinblastine to CaM (cf. Figure 6B, curve c). However, to get a good fit to the experimental points, the affinities of the drugs to the protein within the ternary complex have to be reduced, indicating that the two drugs mutually weaken their binding to CaM (K_d for KAR-2 binding to the CaM−vinblastine complex is 15.3 ± 3.2 μM). This observation resembles our earlier one (*52*), namely, TFP and an aryl-alkylamine derivative (KHL-8430) bind simultaneously to CaM but with reduced affinity as compared to the binary complexes.

Previously, we suggested that the binding of bisindole derivatives to CaM requires dimeric (catharanthine plus vindoline moieties) structure and that the catharantine moiety is essential for the interaction with CaM (*23*). The structures of KAR-2 and vinblastine are identical in the catharantine part; however, the vindoline moiety of KAR-2 is derived by a substituted oxazolidino ring, closed across the two C-3 substituents. This derivation does not influence significantly the ability of KAR-2 to be complexed with CaM. Nevertheless, as demonstrated by the present spectroscopic data, the binding domains on the surface of CaM seem to be at least partially different, although an overlap between these domains is possible due to the similar ligand structures. This structural arrangement could explain, on one hand, that the two bisindoles interact simultaneously with CaM but with reduced affinity, and on the other hand, how the two drugs can display such different anti-CaM activity in the phosphofructokinase assay (*23*, *26*). Indeed, we have suggested that the "extra ring" of the vindoline moiety which occurs in KAR-2 but not in vinblastine is responsible for the lack of anti-CaM potency; it probably makes KAR-2 unable to compete with phosphofructokinase for CaM binding. The binding data from this section and the recent functional data are also included in Scheme 1. The combination of CD and fluorescence measurements suggests that binding domains of the first TFP and vinblastine counteract each other at the C-terminal pocket while KAR-2 may compete with the second TFP for the binding to one of two interdomain sites.

Melittin and Drugs. Melittin is frequently used to study the structural and functional behavior of CaM. This peptide is considered to be analogous to the binding domain of target enzymes. It binds to the protein with a nanomolar dissociation constant because multiple intra- and interdomain sites are involved in the CaM−peptide interaction. To reveal how the drugs, TFP and bisindoles, interfere with melittin for CaM binding, differential CD spectroscopic measurements were carried out. Experimental conditions were identical to those

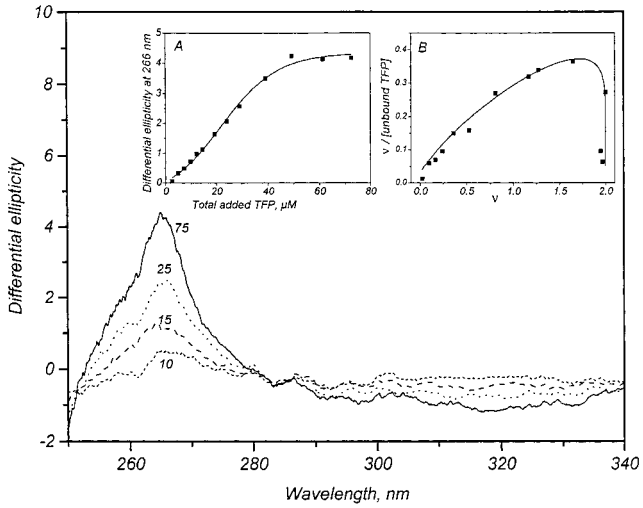

FIGURE 7: Ternary complex of CaM with melittin and TFP. Difference spectra of the 1:1 CaM−melittin complex (21 μM) with TFP (0−75 μM). (Inset A) Cooperative binding of TFP to the melittin−CaM complex. The sigmoidal change in the difference peak at 266 nm is a function of TFP concentration**.** The solid line is the best fit to the Boltzmann equation $\Delta\Theta = (\Delta\Theta_{initial} - \Delta\Theta_{final})/\{1 + \exp(([TFP] - [TFP]_{0.5})/dx)\} + \Delta\Theta_{final}$, where $\Delta\Theta$ is the differential ellipticity at 266 nm as shown on the ordinate, $\Delta\Theta_{initial}$ (= −0.52 mdeg) is $\Delta\Theta$ at [TFP] = 0, $\Delta\Theta_{final}$ (=4.3 mdeg) is $\Delta\Theta$ at saturation, [TFP] is the TFP concentration as shown on the abscissa, $[TFP]_{0.5}$ (=21.9 μM) is [TFP] at half-maximal $\Delta\Theta$, and dx (=10.9) is the width of the Boltzmann curve. (Inset B) Scatchard plot computed from the data of inset A. The molar concentration of bound TFP was calculated from the difference peak at 266 nm with the value of 101 deg/M/cm molar ellipticity for the complex. The solid line (theoretical curve) was obtained by using the equation $\ln [L] = -(1/\alpha_H) \ln [(n/\nu) - 1] + \ln K$, where [L] = concentration of uncomplexed TFP, α_H = Hill constant, n = number of binding sites, ν = number of TFP bound per macromolecule, and K = apparent dissociation constant for the interacting sites. The parameters estimated from the linearized plot (not shown) (α_H = 1.5, n = 2, K = 30 μM) were used to generate the theoretical curve.

used in the studies without melittin where the addition of TFP up to 80 μM concentration induced characteristic and consecutive negative and positive CD signals (cf. Figure 2A). The method is expected to be efficient even in this complex system since the CD signals in the near-UV range elicited by melittin binding to the CaM at the concentrations used in our experiments are beyond the detection limit (data not shown; cf. also refs *28* and *50*).

In one set of experiments the CaM−melittin complex was titrated with TFP, and the binding of the drug was followed in the near-UV range (Figure 7). The difference spectrum is considerably altered as compared to the experiment without melittin (cf. Figure 2A). This finding is evidence for the simultaneous association of the two different ligands (melittin and TFP) on the protein. The negative peak characteristic to the occupation of the C-terminal pocket with TFP completely disappeared. Instead, a complex positive peak with a maximum at 266 nm—close to the location of the positive peak measured without melittin—appeared from the begining of the titration, and the extent but not the shape of this signal was changed by the addition of TFP. Inset A to Figure 7 shows saturable behavior of the characteristic difference peak at 266 nm. Interestingly, the binding curve is clearly sigmoidal in contrast to the simple hyperbolic saturation found in the absence of melittin (cf. Figure 2A, inset). The sigmoid saturation curve suggests positive

Table 1: Ternary Complexes of CaM with Two Different Ligands

components in addition to CaM	ternary complex formation	method, ref
melittin + TFP	yes	CD (Figure 7), *18*
melittin + KAR-2	no	CD (data in text)
melittin + vinblastine	no	CD (data in text)
KAR-2 + TFP	yes	CD (Figure 5)
vinblastine + TFP	no	CD (Figure 5)
vinblastine + KAR-2	yes	fluorescence (Figure 6)

cooperativity in the binding of the TFP molecules to the melittin−CaM complex: the association of the first TFP to the protein−peptide complex enhances the binding of additional TFP molecule(s). To quantify this cooperativity, data were plotted in the conventional Scatchard plot (Figure 7, inset B) using 2:1 stoichiometry for TFP:CaM−melittin complex as suggested by Massom et al. (*18*): the Hill coefficient estimated from the titration curve was 1.5. We conclude that these data reinforce the formation of the melittin−TFP_2−CaM complex and suggest communication between the protein-bound TFP molecules. As to the identification of the TFP sites available in the melittin−CaM complex as intradomain or interdomain sites, the negative peak at 263 nm, characteristic for the C-terminal intradomain site, is completely erased. The positive difference peak at 266 nm of the ternary complex is reminescent of the second-to-appear peak in the TFP−CaM complex (Figure 2A) which was suggested to reflect saturation of interdomain sites. This interpretation is in agreement with the earlier data of Steiner et al. (*50*), whose results on the exclusive competion between TFP and melittin for trypsinolyzed CaM provided evidence for the essential role of unharmed interdomain contacts for the formation of the ternary complex. The possibility that TFP molecule(s) interact directly with melittin in the ternary CaM−melittin−TFP complex cannot be excluded. However, even if this were the case, the role of the central linker region is indispensable for the simultaneous interaction of CaM with melittin and TFP.

In other sets of experiments vinblastine or KAR-2 was added to the CaM−melittin complex, and the formation of the differential CD signal was followed just as in the control (no melittin) experiments. We found that the presence of melittin practically erased the differential CD signal characteristic for the binding of either vinblastine or KAR-2 (data not shown). The simplest explanation of these observations is that bisindoles are not able to interact with the CaM−melittin complex.

Distinct Protein Conformers Induced by Different CaM−Drug Complexes. The results obtained for multiple ligand bindings are summarized in Table 1. The following considerations are proposed to account for the lack or existence of ternary complexes. Vinblastine and the first TFP molecule likely bind alternatively to the C-terminal hydrophobic pocket. Therefore, their dissociation constants as well as their concentrations determine the dominance of the binary complexes. KAR-2 and the second TFP molecule apparently interact with an interdomain site at the long central region of the CaM; thus the ternary CaM−$TFP_{C-terminal}$−KAR-2 complex can be formed. Cross-talk between the KAR-2 site and the C-terminal TFP site may occur (enhanced TFP-specific CD signal in Figure 5A,C). From this arrangement it is not surprising that the two bisindoles can simultaneously

bind on CaM; however, each mutually weakens the binding of the other. This hypothesis is justified by the data of fluorescence measurements. Therefore, long-distance interactions could create effective communication between these different binding domains of the intact CaM which finally determine which binary or ternary CaM complexes will be formed.

Melittin binding displaces both vinblastine from its C-terminal intradomain site and KAR-2 from its interdomain site due to the fact that the peptide occupies all of these sites. However, two molecules of TFP still find some contacts with the CaM−melittin complex. The altered difference spectra and the cooperative behavior (Figure 7 as compared to Figure 2A) suggest that these two TFP molecules are bound to different sites than in intact CaM.

The X-ray and spectroscopic data obtained for CaM−drug complexes are also important to understand the structural basis for the functional effect of CaM in the absence and presence of drugs. TFP is a classic CaM antagonist: it competes with the binding of the target enzyme to CaM, probably at the C-terminal hydrophobic pocket. The two bisindole drugs, vinblastine and KAR-2, display different functional effects: while vinblastine behaves as a CaM antagonist, KAR-2 is inactive in the CaM−PFK system (*23*, *26*). These functional consequences of drug binding to CaM are in good agreement with the expectations from the structural data of Scheme 1, emphasizing the critical role of the occupation of the C-terminal intradomain site. The fact that TFP displays different binding patterns to CaM fragments, to intact CaM, and to the CaM−melittin complex indicates the complexity of the interaction of CaM with this drug. On the other hand, the association of melittin, considered as a target peptide analogue, prevents the binding of both bisindoles, but not that of TFP, to CaM. This may suggest that if CaM is complexed with a target peptide/enzyme, then the binding of different drugs can create CaM conformers with altered functional effects. This idea, based on the present studies, helps in understanding the multifarious character of CaM which is responsible for its stimulating/inhibitory effects. Moreover, our data are relevant from a pharmacological point of view since they could assist in the design of selective anti-CaM drugs.

ACKNOWLEDGMENT

The excellent technical assistance of Ms. Emma Hlavanda is gratefully acknowledged. B.G.V. thanks Dr. Eila Cedergren-Zeppezauer for her kind help in the preliminary crystallization trials.

REFERENCES

1. Crivici, A., and Ikura, M. (1995) *Annu. Rev. Biophys. Biomol. Struct. 24*, 85−115.
2. James, P., Vorherr, T., and Carafoli, E. (1995) *Trends Biochem. Sci. 20*, 38−42.
3. Mayr, G. W. (1987) *Methods Enzymol. 139*, 745−763.
4. Orosz, F., Christova, T. Y., and Ovadi, J. (1988) *Biochim. Biophys. Acta 957*, 293−300.
5. Babu, Y. S., Bugg, C. E., and Cook, W. J. (1988) *J. Mol. Biol. 204*, 191−204.
6. Chattopadhyaya, R., Meador, W. E., Means, A. R., and Quiocho, F. A. (1992) *J. Mol. Biol. 228*, 1177−1192.
7. Taylor, D. A., Sack, J. S., Maune, J. F., Beckingham, K., and Quiocho, F. A. (1991) *J. Biol. Chem. 266*, 21375−21380.
8. Barbato, G., Ikura, M., Kay, L. E., Pastor, R. W., and Bax, A. (1992) *Biochemistry 31*, 5269−5278.
9. Heidorn, D. B., and Trewhella, J. (1988) *Biochemistry 27*, 909−915.
10. Walsh, M., Stevens, F. C., Kuznicki, J., and Drabikowski, W. (1977) *J. Biol. Chem. 252*, 7440−7443.
11. Ikura, M., Clore, G. M., Gronenborn, A. M., Zhu, G., Klee, C. B., and Bax, A. (1992) *Science 256*, 632−638.
12. Meador, W. E., Means, A. R., and Quiocho, F. A. (1992) *Science 257*, 1251−1255.
13. Meador, W. E., Means, A. R., and Quiocho, F. A. (1993) *Science 262*, 1718−1721.
14. Cook, W. J., Walter, L. J., and Walter, M. R. (1994) *Biochemistry 33*, 152590−15265.
15. Vandonselaar, M., Hickie, R. A., Quail, J. W., and Delbaere, L. T. J. (1994) *Nat. Struct. Biol. 1*, 795−801.
16. Levin, R. M., and Weiss, B. (1978) *Biochim. Biophys. Acta 540*, 197−204.
17. Marshak, D. R., Lukas, T. J., and Watterson, D. M. (1985) *Biochemistry 24*, 144−150.
18. Massom, L., Lee, H., and Jarrett, H. W. (1990) *Biochemistry 29*, 671−681.
19. DeLaLuz, P. J., Golinski M., Watt, D. S., and Vanaman, T. C. (1995) *Bioconjugate Chem. 6*, 558−588.
20. Faust, F. M., Slisz, M., and Jarrett, H. W. (1987) *J. Biol. Chem. 262*, 1938−1941.
21. Klevit, R. E., Levine, B. A., and Williams, R. J. P. (1981) *FEBS Lett. 123*, 25−29.
22. Orosz, F., Christova, T. Y., and Ovádi, J. (1988) *Mol. Pharmacol. 33*, 678−682.
23. Molnár, A., Liliom, K., Orosz, F., Vertessy, B. G., and Ovádi, J. (1995) *Eur. J. Pharmacol. 291*, 73−82.
24. Ovádi, J., Keve, T., Ács, T., Orosz, F., Lehotzky, A., Liliom, K., Molnár, A., Nuridsány, M., Hlavanda, E., Vertessy, B. G., Kovács, J., and Löw, M. (1995) Hungarian Patent Description 978/95.
25. Watabene, K., and West, U. (1981) *Biochem. Pharmacol. 30*, 335−340.
26. Orosz, F., Vertessy, B. G., Salerno, C., Crifo, C., Capuozzo, E., and Ovádi, J. (1997) *Br. J. Pharmacol. 121*, 955−962.
27. Vertessy, B. G., Böcskei, Zs., Harmath, V., Náray-Szabó, G., and Ovádi, J. (1997) *Proteins 28*, 131−134.
28. Orosz, F., Kovács, J., Löw, P., Vertessy, B. G., Urbányi, Z., Ács, T., Keve, T., and Ovádi, J. (1997) *Br. J. Pharmacol. 121*, 947−954.
29. Maulet, Y., and Cox, J. A. (1983) *Biochemistry 22*, 5680−5686.
30. Malencik, D. A., and Anderson, S. R. (1984) *Biochemistry 23*, 2420−2428.
31. Seeholzer, S. H., Cohn, M., Putkey, J. A., Means, A. R., and Crespi, H. L. (1986) *Proc. Natl. Acad. Sci. U.S.A. 83*, 3634−3638.
32. Steiner, R. F., Albaugh, S., Fenselau, C., Murphy, C., and Vestling, M. (1991) *Anal. Biochem. 196*, 120−125.
33. Itakura, M., and Iio, T. (1992) *J. Biochem. (Tokyo) 112*, 183−191.
34. Orosz, F., Liliom, K., Barkhudaryan, N., Horváth, L., and Ovádi, J. (1992) *Biochem. J. 284*, 803−808.
35. Gopalakrisha, R., and Anderson, W. B. (1982) *Biochem. Biophys. Res. Commun. 104*, 830−836.
36. Laemmli, U. K. (1970) *Nature 227*, 680−688.
37. Watterson, D. M., Harrelson, W. G., Keller, P. M., Sharief, F., and Vanaman, T. C. (1976) *J. Biol. Chem. 251*, 4501−4513.
38. Lakowicz, J. R. (1983) *Principles of Fluorescence Spectroscopy*, Plenum Press, New York.
39. BioteX, Version 1.0 (1995) Molecular Structure Corporation, The Woodlands, TX.
40. Navaza, J. (1994) *Acta Crystallogr. A50*, 157−163.
41. Jones, T. A., Zou, J.-Y., Cowan, S. W., and Kjeldgaard, M. (1991) *Acta Crystallogr. A47*, 110−119.
42. Brunger, A. T. (1992) X-PLOR Version 3.851, Yale University, New Haven, CT.
43. Bae, D.-S., and Haug, E. J. (1987) *Mech. Struct. Mach. 15*, 359−382.

44. Bae, D.-S., and Haug, E. J. (1988) *Mech. Struct. Mach. 15*, 481−506.
45. Rice, L. M., and Brunger, A. T. (1994) *Proteins 19*, 277−290.
46. Brunger, A. T., Kuriyan, J., and Karplus, M. (1987) *Science 235*, 458−460.
47. Brunger, A. T., Krukowski, A., and Erickson, J. (1990) *Acta Crystallogr. A46*, 585−593.
48. Brunger, A. T. (1992) *Nature 355*, 472−474.
49. Jiang, J.-S., and Brunger, A. T. (1994) *J. Mol. Biol. 243*, 100−115.
50. Steiner, R. F., Marshall, L., and Needleman, D. (1986) *Arch. Biochem. Biophys. 246*, 286−300.
51. Johnson, J. D., and Wittenauer, L. A. (1983) *Biochem. J. 211*, 473−479.
52. Orosz, F., Telegdi, M., Liliom, K., Solti, M., Korbonits, D., and Ovádi, J. (1990) *Mol. Pharmacol. 38*, 910−916.
53. Cantor, C. R., and Schimmel, P. R. (1980) *Biophysical Chemistry*, Chapter 15, pp 849−886, W. H. Freeman and Co., San Francisco.
54. Wang, Z.-X. (1995) *FEBS Lett. 360*, 111−114.

BI980795A